Processing and Application of Ceramics 15 [3] (2021) 297–305
https://doi.org/10.2298/PAC2103297Z

Effect of particle size of Y_2O_3-Al_2O_3 additives on microstructure and mechanical properties of Si_3N_4 ceramic balls for bearing applications

Jing Zhang[1,*], Wenxue Wang[2], Feng Sun[1], Weiru Zhang[1,3], Boheng Li[2], Mingshuai Zhang[2]

[1]*Sinoma Advanced Nitride Ceramics Co. Ltd, Zibo 255000, China*
[2]*AECC Harbin Bearing Co. Ltd, Harbin 150025, China*
[3]*Shandong Industrial Ceramic Research and Design Institute Co. Ltd, Zibo 255000, China*

Received 22 April 2021; Received in revised form 11 August 2021; Accepted 3 July 2021

Abstract

Si_3N_4 ceramic balls were prepared by gas pressure sintering with Y_2O_3 and Al_2O_3 as sintering additives. The effects of particle size of Y_2O_3-Al_2O_3 additives on densification, microstructure and mechanical properties of Si_3N_4 ceramic balls were investigated. The reliability of Si_3N_4 ceramic balls was evaluated through the Weibull modulus. The results showed that Si_3N_4 ceramic balls containing nanosized Y_2O_3-Al_2O_3 additives have a higher relative density and better comprehensive mechanical properties compared with the samples containing microsized additives, with relative density of 98.9 ± 0.2% TD, Vickers hardness of 14.7 ± 0.1 GPa, indentation fracture toughness of 6.5 ± 0.1 MPa·$m^{1/2}$ and crushing strength of 254 ± 8.5 MPa. The more homogeneous and extensive dispersion of the nanosized sintering additives in the Si_3N_4 matrix is the main reason for the enhancement in density and mechanical properties of the Si_3N_4 ceramic balls.

Keywords: *ceramic balls, Si_3N_4, nanosized sintering additives, microstructure, mechanical properties*

I. Introduction

Silicon nitride (Si_3N_4) ceramics have excellent properties such as high strength, high hardness, wear resistance, heat resistance, electrical insulation and self-lubrication, which is an ideal material for rolling elements used in bearings [1,2]. The bearings with Si_3N_4 ceramic balls or rollers are particularly suitable for working under high-speed, cryogenic or high-temperature, low-torque, and oil-lean lubrication conditions, such as spindle bearings in precision machine tools, windmill generator bearings and aerospace bearings [3,4]. Si_3N_4 is a compound with strong covalent bond and low self-diffusion coefficient. Therefore, it is necessary to add sintering additives during sintering to complete the densification by means of liquid phase sintering [5]. Sintering additives react with the native SiO_2 on the surface of Si_3N_4 particles to form a liquid phase, in which densification and grain growth are achieved through particle rearrangement and dissolution-reprecipitation mechanisms [6]. The sintering additives for Si_3N_4 ceramics include Y_2O_3, Al_2O_3, MgO, AlN, La_2O_3, etc. In order to decrease the formation temperature of liquid phase and tailor the chemical composition of grain boundary phase, binary or multiple sintering additive systems are commonly used [7–10].

The sintering methods of Si_3N_4 ceramics include pressureless sintering, gas pressure sintering (GPS), hot pressing (HP), hot isostatic pressing (HIP), spark plasma sintering (SPS), etc. [10–16,25]. Si_3N_4 would decompose above 1700 °C under atmospheric pressure, hence the powder bed technology is conventionally used during pressureless sintering to inhibit the decomposition of Si_3N_4. In order to decrease the firing temperature of pressureless sintering and promote densification, a large amount of sintering additives (usually ≥10 wt.%) is added, which significantly degrades the high-temperature performance of products [10,11]. Hot pressing is a technology by which the densification of sintered body is realized under the dual action of liquid phase and mechanical pressure. The properties of hot-pressed Si_3N_4 ceramics are excellent. However, due to the limitation of graphite die, hot pressing could only produce the components with simple shapes [12]. Although hot isostatic pressing could fabricate complex-

*Corresponding author: tel: +86 18560942738,
e-mail: *zhji86@163.com*

structure products, the cost is relatively high [13]. Gas pressure sintering relies on high-pressure nitrogen (1–10 MPa) to retard the decomposition of Si_3N_4, by which the sintering temperature of Si_3N_4 ceramics is able to rise above 1900 °C. Gas pressure sintering resolves the contradiction between densification and high temperature decomposition during sintering of Si_3N_4 ceramics, and it is adapted for batch production [14–16].

Some defects are inevitably introduced in ceramic materials, such as pores or cracks during the preparation process. The uncertainty of the size, number and distribution of defects leads to the discreteness of mechanical properties data of ceramics, especially strength data. Generally, the statistical method based on the Weibull distribution is applied to evaluate the discreteness of strength data of ceramic materials [17–20]. The greater the Weibull modulus of strength data, the higher the reliability. Jayatilaka and Trustrum [17,18] studied the relationship between defect size distribution and the Weibull modulus. They argued that there is a power function relationship between fracture probability and crack size of brittle materials, and proposed that the relationship between the Weibull modulus m and power function exponent n of crack size is $m = 2n - 2$. Nakamura *et al.* [19] investigated the relationship between the distribution of large-size defects in alumina ceramics and the Weibull modulus of flexural strength through numerical simulation and experiment, and the results were consistent with the conclusions of Jayatilaka and Trustrum [17].

In this work, silicon nitride (Si_3N_4) ceramic balls for bearing applications were prepared by gas pressure sintering with both microsized and nanosized Y_2O_3-Al_2O_3 powders as sintering additives. The effects of particle size of Y_2O_3-Al_2O_3 additives on the densification, phase compositions, microstructure and mechanical properties of Si_3N_4 ceramic balls were studied. Moreover, the reliability of gas-pressure-sintered Si3N4 ceramic balls was evaluated based on the Weibull modulus.

II. Experimental

2.1. Materials preparation

The raw materials include Si_3N_4 powder (homemade, α-Si_3N_4 content >93 wt.%, oxygen content <2 wt.%, average particle size is 0.7 μm) and different additives: microsized Y_2O_3 (average particle size is 1.2 μm), microsized Al_2O_3 (average particle size is 0.8 μm), nanosized Y_2O_3 (average particle size is 50 nm) and nanosized Al_2O_3 (average particle size is 30 nm), all purchased from Sinopharm Chemical, China and with purity of >99.9 wt.%.

The Si_3N_4 powder and sintering additives were put into a nylon jar according to the weight ratio of Si_3N_4 : Y_2O_3 : Al_2O_3 = 90 : 5 : 5, with ethanol and Si_3N_4 balls as media for mixing and dispersion. The uniformly mixed slurry was granulated by spray drying, and the granules were mould-pressed into spherical green compacts with a diameter of 9.525 mm under 10 MPa followed by cold isostatic pressing (CIP) under 200 MPa. The cold-isostatically-pressed ceramic ball green compacts were placed in a GPS furnace for sintering. The highest firing temperatures were 1720, 1750, 1780 and 1800 °C, with a holding time of 2 h and nitrogen pressure of 3 MPa. The samples containing the microsized and nanosized sintering additives were marked as samples MSA and NSA, respectively.

2.2. Materials characterization

The bulk density of Si_3N_4 ceramic balls was measured by the Archimedes' method, and the relative density was calculated from the theoretical densities of each raw powder using a linear rule of mixture, as shown in Eq. 1:

$$\rho_{rd} = \frac{\rho_m}{\rho_{th}} \times 100 = \frac{\rho_m}{\sum \rho_i \cdot V_i} \times 100 \tag{1}$$

where ρ_{rd} is the relative density, ρ_m is the bulk density, ρ_{th} is the theoretical density, ρ_i is the theoretical density of each composition and V_i is the volume fraction of each composition.

The phase compositions of the Si_3N_4 ceramic balls were identified by X-ray diffraction (XRD, D8, Bruker, Germany). The microstructure of the Si_3N_4 ceramic balls was observed with a field-emission scanning electron microscope (FESEM, SU8010, Hitachi, Japan). The Vickers hardness was measured on the polished surface of the samples with a load of 98 N. The indentation fracture toughness (196 N load) was determined referring to the calculation Eq. 2 proposed by Niihara *et al.* [21]:

$$K_{I,IFR} = 10.4 \cdot E^{0.4} \cdot L^{0.6} \frac{a^{0.8}}{c^{1.5}} \tag{2}$$

where $K_{I,IFR}$ is the indentation fracture toughness, E is the elastic modulus (here, E = 310 GPa), L is the load, a is the mean half-length of indentation diagonal and c is the mean half-length of tip-to-tip crack.

The crushing load of ceramic balls was tested by triple ball crush method. The schematic of the test setup is shown in Fig. 1 [22]. Calculation of the crushing strength is given in Eq. 3 [23]:

$$\sigma = \frac{F}{d^2} \tag{3}$$

where σ is the crushing strength of ceramc balls, F is the crushing load of ceramic balls and d is the diameter of ceramic balls.

The Weibull function describing the fracture strength distribution of ceramic materials is as follows [20]:

$$P = 1 - \exp\left[-\left(\frac{\sigma}{\sigma_0}\right)^m\right] \tag{4}$$

where P is the fracture probability, σ_0 is the character-

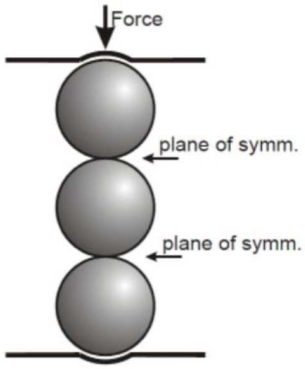

Figure 1. Schematic of testing setup for a triple ball crush test [22]

istic fracture strength and m is the Weibull modulus.

It can be seen from Eq. 4 that $\ln\ln[1/(1-P)]$ has a linear relationship with $\ln\sigma$ and the slope of the straight line is the Weibull modulus. In the present work, the reliability of Si_3N_4 ceramic balls is evaluated by the Weibull modulus of crushing strength. 15 groups of crushing strength data were tested for the ceramic balls and the test results were arranged in a sequence from small to large. The fracture probability P_i of the ceramic balls under the external load not higher than σ_i is as follows:

$$P_i = \frac{i - 0.5}{n} \tag{5}$$

where i is the ranking and n is the number of groups of samples tested (here, $n = 15$).

According to Eq. 5, 15 groups of (P_i, σ_i) data could be obtained and the Weibull modulus of crushing strength distribution of the Si_3N_4 ceramic balls could be estimated through linear regression analysis on the 15 groups of (P_i, σ_i) data using least squares method.

III. Results and discussion

3.1. Densification

Figure 2 shows the relative density and weight loss of the Si_3N_4 ceramic balls with the microsized and nanosized sintering additives sintered at 1720, 1750, 1780 and 1800 °C. It can be seen from Fig. 2a that the relative density of both samples NSA and MSA initially increases and then decreases with an increase in sintering temperature. The viscosity of liquid phase is decreased and mass diffusion is enhanced due to the increase of sintering temperature, which could accelerate the growth of Si_3N_4 grains and elimination of pores [24]. As a result, the density of the sintered body is increased.

However, when the sintering temperature is too high, a decrease in the relative density emerges for both samples NSA and MSA. The metallographic images of the sample NSA at different sintering temperatures are shown in Fig. 3. It can be seen from Fig. 3 that the percentage of micropores in the sintered body increases at a firing temperature higher than 1750 °C, attributed to the raising of the weight loss caused by decomposition of Si_3N_4 or volatilization of liquid phase [25]. A similar phenomenon was also observed for the sample MSA (metallographic images are not shown here). Consequently, the density is decreased.

The sintering temperatures when the highest relative density is achieved for the samples NSA (98.9 ± 0.2% TD) and MSA (98.6 ± 0.3% TD) are 1750 and 1780 °C, respectively, indicating that the nanosized sintering additives could promote the densification of the Si_3N_4 ceramic balls at a slightly lower temperature. The dispersion of sintering additives with various particle sizes in Si_3N_4 matrix is different. The finer the particle size of sintering additives, the more uniform their dispersion in Si_3N_4 matrix is. On the contrary, when the particle size of sintering additives is coarser, the distribution of sintering additives tends to be more agglomerated [26,27]. The homogeneous distribution of liquid phase contributes to the wrapping and wetting of Si_3N_4 particles, thus the particles rearrangement and solution-reprecipitation process are enhanced. Meanwhile, the nanosized additives would produce a liquid phase earlier than microsized additives during sintering, which is also beneficial to the densification of Si_3N_4 ceramic balls at a lower temperature.

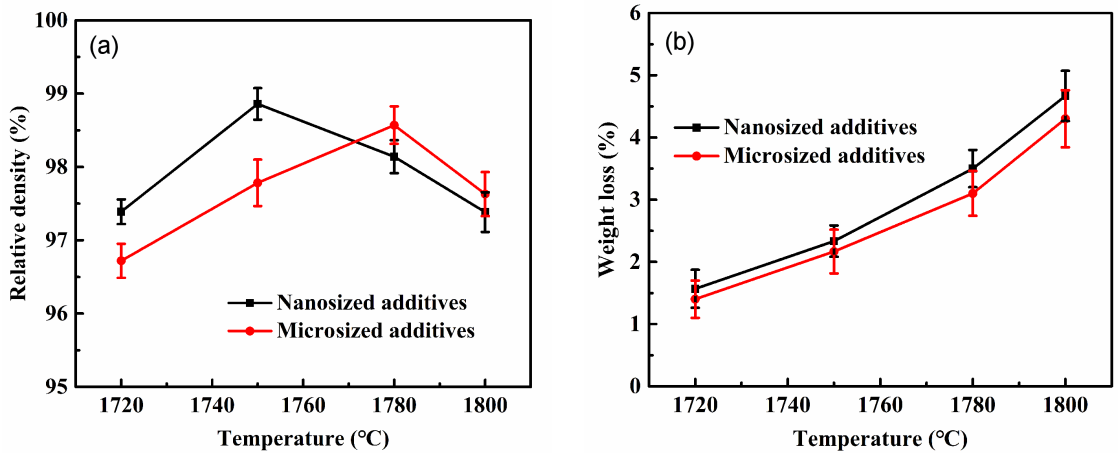

Figure 2. The relative density and weight loss of Si_3N_4 ceramic balls

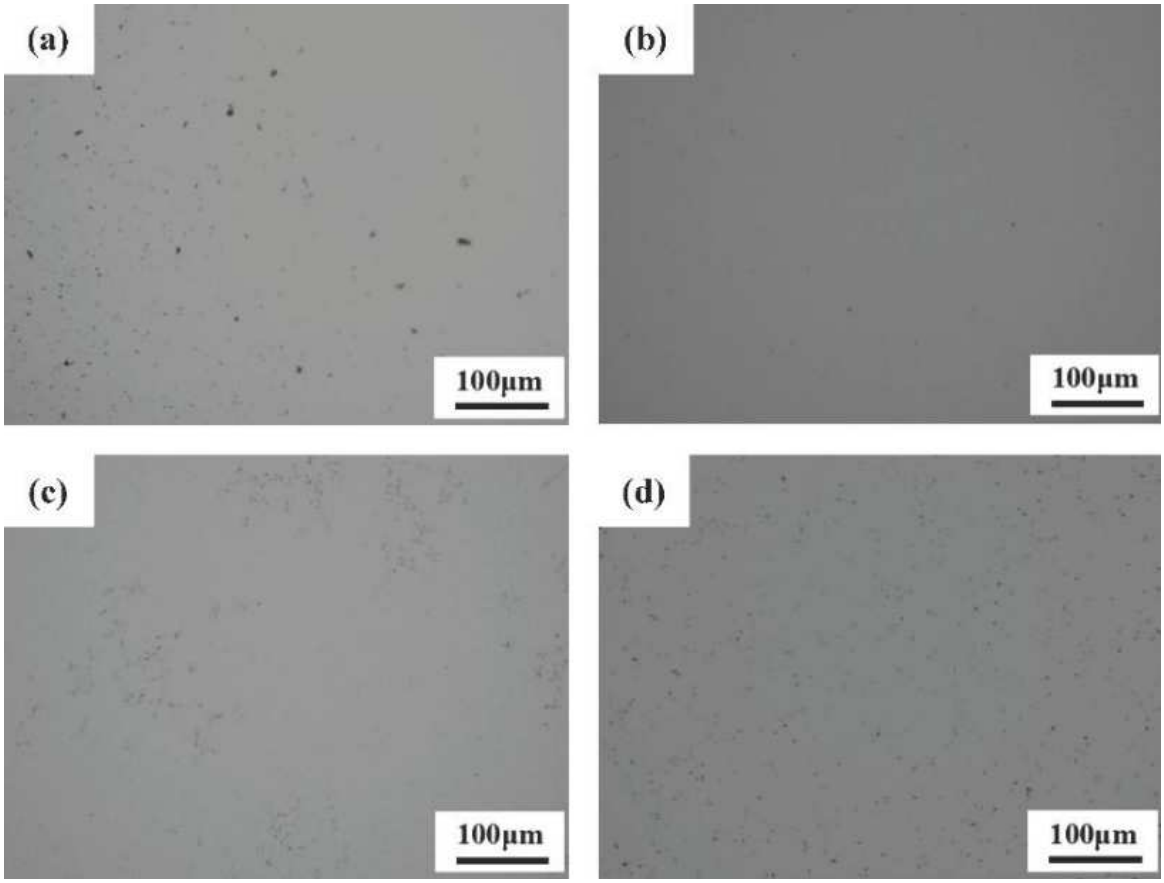

Figure 3. Metallographic images of sample NSA at different sintering temperatures: a) 1720, b) 1750, c) 1780 and d) 1800 °C

3.2. Phase compositions

Figure 4 shows XRD patterns of the Si_3N_4 starting powder and Si_3N_4 ceramic balls with the microsized and nanosized sintering additives sintered at 1720 °C. It can be seen from Fig. 4 that only diffraction peaks of β-Si_3N_4 exist in the XRD patterns for the samples NSA and MSA, which indicates that the phase transformation of α-Si_3N_4 to β-Si_3N_4 has been completed at 1720 °C for both samples. The diffraction peaks of grain boundary phases formed from sintering additives were not observed in the XRD patterns, because they may be below the detection limit of XRD or they remained as amorphous phase in the samples.

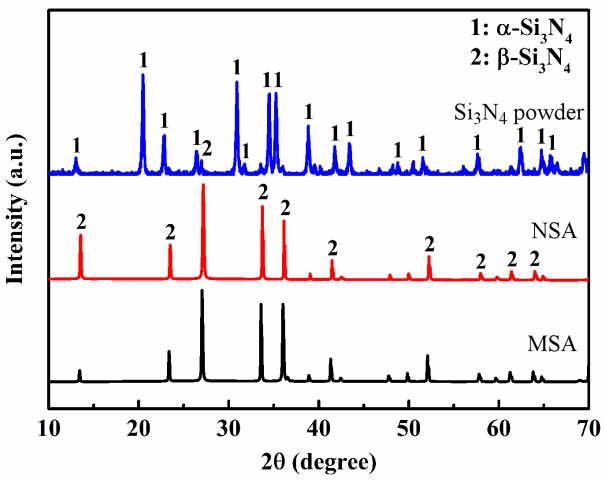

Figure 4. XRD patterns of Si_3N_4 powder, sample NSA and sample MSA

3.3. Microstructure

Figures 5 and 6 are SEM images of the Si_3N_4 ceramic balls sintered at different temperatures with the nanosized and microsized sintering additives, respectively. Statistics on the diameter and aspect ratio of β-Si_3N_4 grains for the samples NSA and MSA are shown in Table 1. It can be seen from Table 1 that both the average grain diameter and aspect ratio of both samples NSA and MSA increase with increasing sintering temperature. The aspect ratio of the sample NSA is larger than that of the sample MSA under the same sintering process parameters, suggesting that the coarsening of sintering additives particles resulted in a decrease in the aspect ratio of β-Si_3N_4 grains. The liquid phase would be formed from the nanosized additives at a lower temperature, which enhanced the α/β phase transformation and the growth of β-Si_3N_4 grains along the length. Consequently, more elongated β-Si_3N_4 grains were developed for the Si_3N_4 ceramic balls with the nanosized Y_2O_3-Al_2O_3 additives.

The distributions of β-Si_3N_4 grain diameter for the samples NSA and MSA at various temperatures are shown in Figs. 7 and 8, respectively. It can be seen from

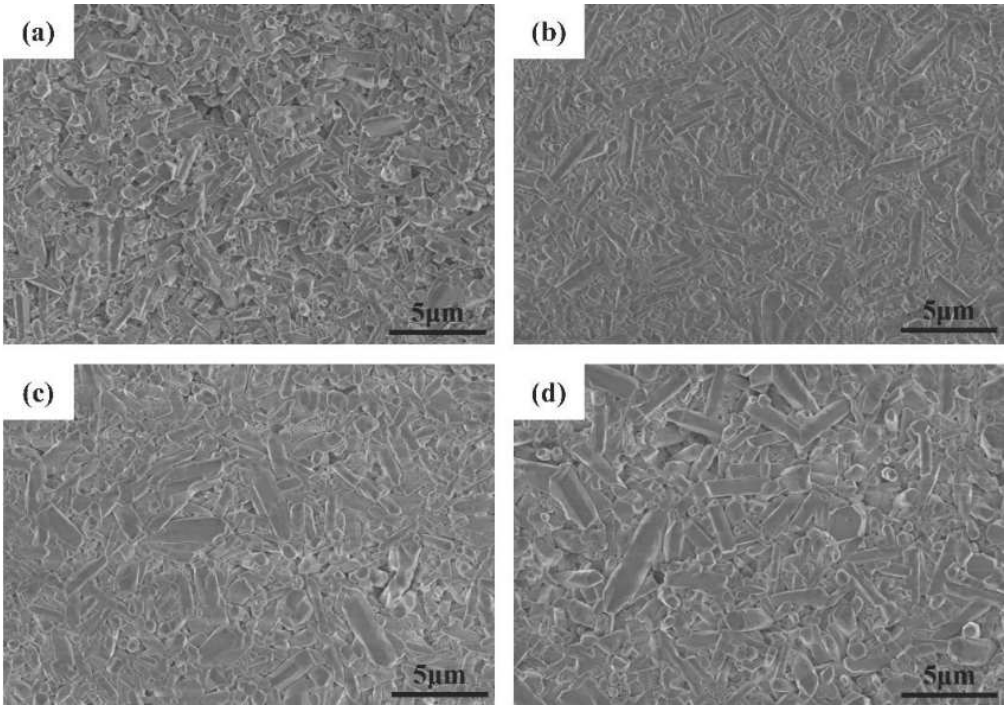

Figure 5. SEM images of Si_3N_4 ceramic balls with nanosized sintering additives sintered at various temperatures: a) 1720, b) 1750, c) 1780 and d) 1800 °C

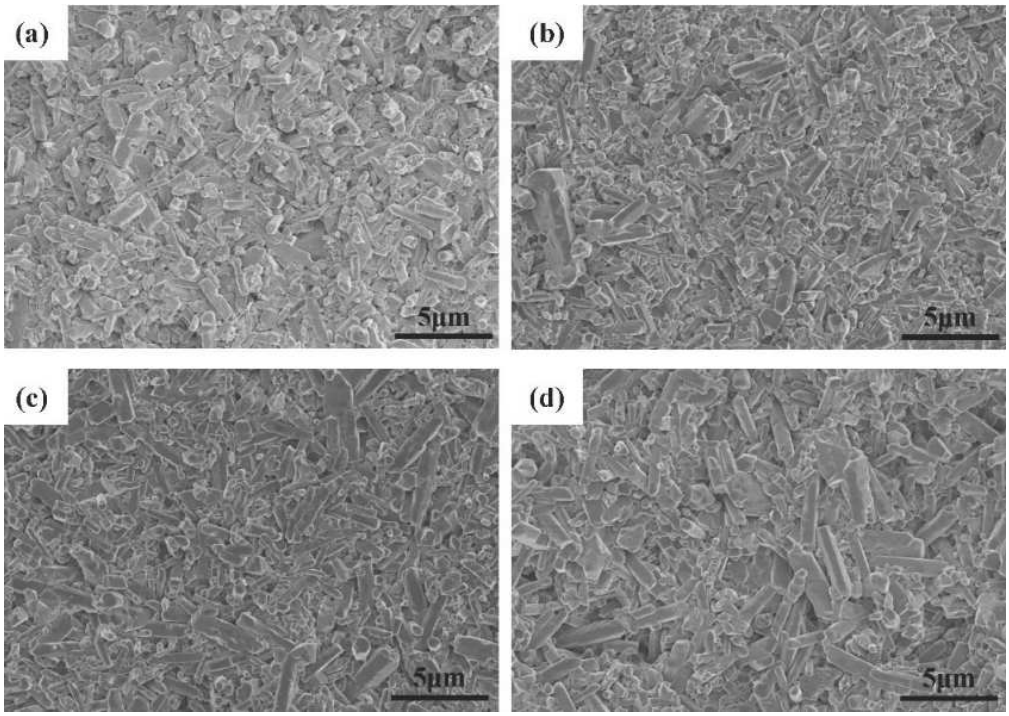

Figure 6. SEM images of Si_3N_4 ceramic balls with microsized sintering additives sintered at various temperatures: a) 1720, b) 1750, c) 1780 and d) 1800 °C

Table 1. Statistics on the average diameter and aspect ratio of β-Si_3N_4 grains for samples NSA and MSA

Temperature [°C]	Sample NSA		Sample MSA	
	Average diameter [μm]	Aspect ratio	Average diameter [μm]	Aspect ratio
1720	0.44 ± 0.12	3.5 ± 1.1	0.43 ± 0.18	3.1 ± 1.5
1750	0.54 ± 0.15	4.8 ± 2.3	0.55 ± 0.25	3.9 ± 2.2
1780	0.65 ± 0.30	5.4 ± 2.8	0.67 ± 0.29	4.5 ± 2.6
1800	0.77 ± 0.31	5.9 ± 2.5	0.76 ± 0.35	5.2 ± 3.0

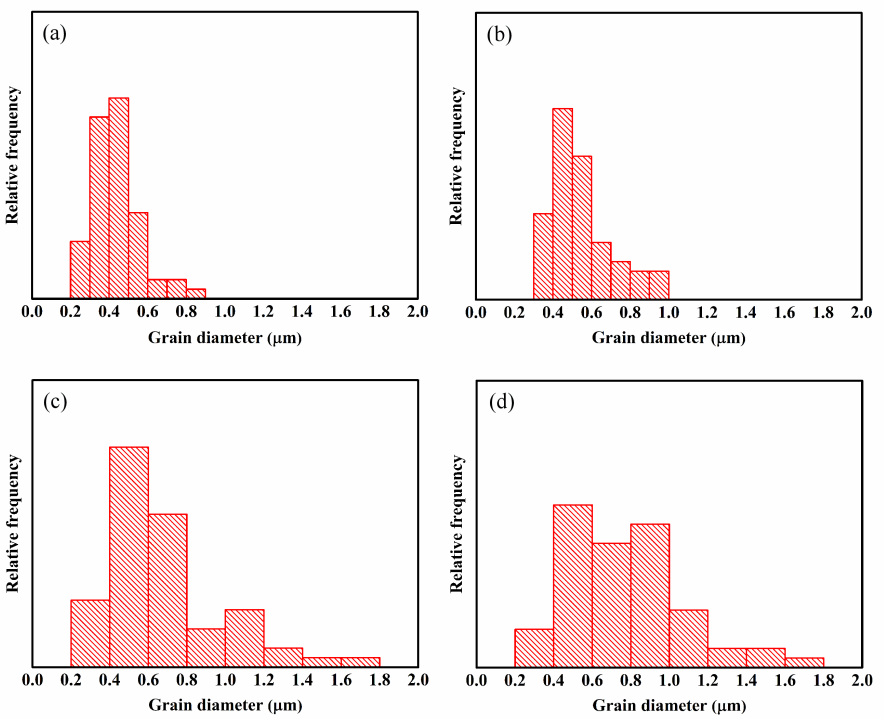

Figure 7. Distribution of β-Si_3N_4 grain diameter in sample NSA at different temperatures: a) 1720, b) 1750, c) 1780 and d) 1800 °C

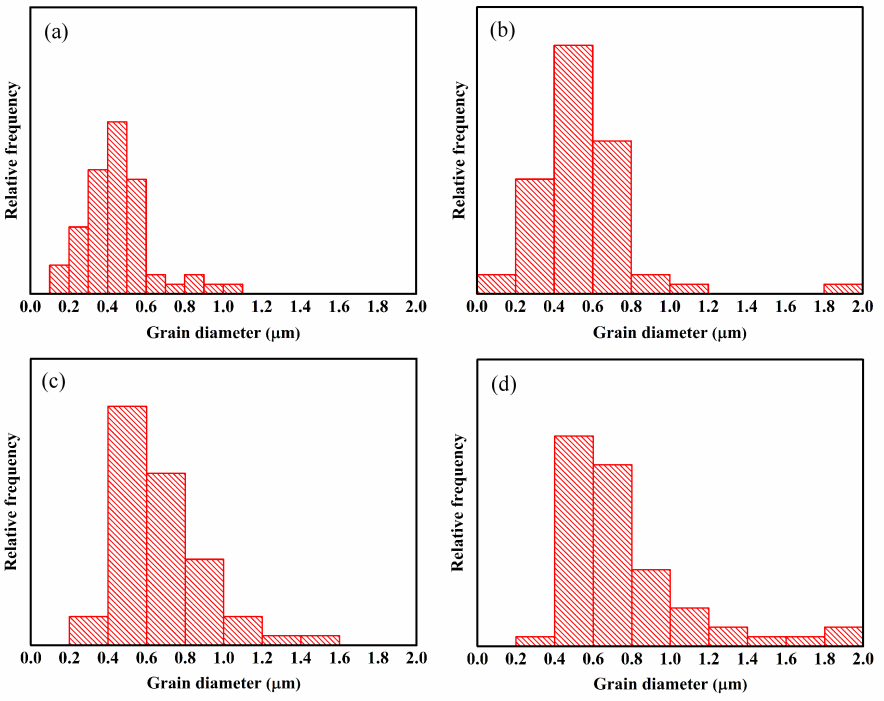

Figure 8. Distribution of β-Si_3N_4 grain diameter in sample MSA at different temperatures: a) 1720, b) 1750, c) 1780 and d) 1800 °C

the comparison of Figs. 7 and 8 that the grain diameter distribution of the sample NSA is more uniform. During sintering, the α- to β-Si_3N_4 phase transformation is completed through the dissolution of equiaxed α-Si_3N_4 grains in the liquid phase and precipitation of β-Si_3N_4 nucleus when the supersaturation is reached. After the phase transformation, the anisotropic growth of β-Si_3N_4 grains will be realized via Ostwald ripening mechanism. The local preferential trend exists in the process of phase transformation, mass transport and β-Si_3N_4 grain growth, owing to the inhomogeneous distribution of the liquid phase generated by the microsized Y_2O_3-Al_2O_3 additives in the Si_3N_4 matrix during the initial stage of sintering [26,27]. In contrast, the nano-

sized sintering additives with high specific surface area would be more widely and evenly dispersed at the interface of the Si_3N_4 matrix, and it is easier to form a uniformly distributed liquid phase under the same conditions [28]. Therefore, a more homogeneous microstructure was obtained for the Si_3N_4 ceramic balls with the nanosized additives.

3.4. Mechanical properties

Figure 9 shows the mechanical properties of the Si_3N_4 ceramic balls with the microsized and nanosized sintering additives after sintering at different temperatures. It can be seen from Fig. 9 that with the increase of sintering temperature, the Vickers hardness and crushing strength of both samples NSA and MSA initially increase and then decrease, but the indentation fracture toughness increases monotonically. The hardness of the Si_3N_4 is related to the content of α-Si_3N_4 phase, the relative density and the characteristics of grain boundary phase [29]. Higher α-Si_3N_4 content, lower porosity and less grain boundary phase are beneficial to improve the hardness of the Si_3N_4 ceramic balls. The α- to β-Si_3N_4 phase transformation has been completed at 1720 °C for both samples, as shown in Fig. 4. Therefore, the main factors that determine the Vickers hardness of the samples are the relative density and characteristics of grain boundary phase.

According to the Griffith theory of fracture, the relationship between fracture strength and defect size is [30]:

$$\sigma = \left(\frac{2E \cdot \gamma}{\pi \cdot c}\right)^{1/2} \tag{6}$$

where σ is the fracture stress, E is the elastic modulus, γ is the fracture energy and c is the defect (e.g. pore, crack, and inclusion) size.

It can be seen from Eq. 6 that when elastic modulus and fracture energy are constant, the fracture strength is inversely proportional to the defect size. Therefore, the variations of the Vickers hardness and crushing strength of the samples NSA and MSA are basically consistent with that of relative density. When the sintering temperature is 1750 °C, a higher relative density is obtained for the sample NSA, due to the more uniform dispersion of the nanosized sintering additives in the Si_3N_4 matrix and lower formation temperature of liquid phase. Consequently, the Vickers hardness and crushing strength of the sample NSA are higher than that of the sample MSA at 1750 °C.

The indentation fracture toughness of Si_3N_4 is affected by the grain size and aspect ratio of β-Si_3N_4 grains and chemical properties of grain boundary phase [14–16]. The grain diameter and aspect ratio of both samples (NSA and MSA) increase with firing temperature, thus the indentation fracture toughness of both samples increases. The sample NSA has a greater grain aspect ratio compared with the sample MSA at the same sintering temperature, resulting in higher indentation fracture toughness.

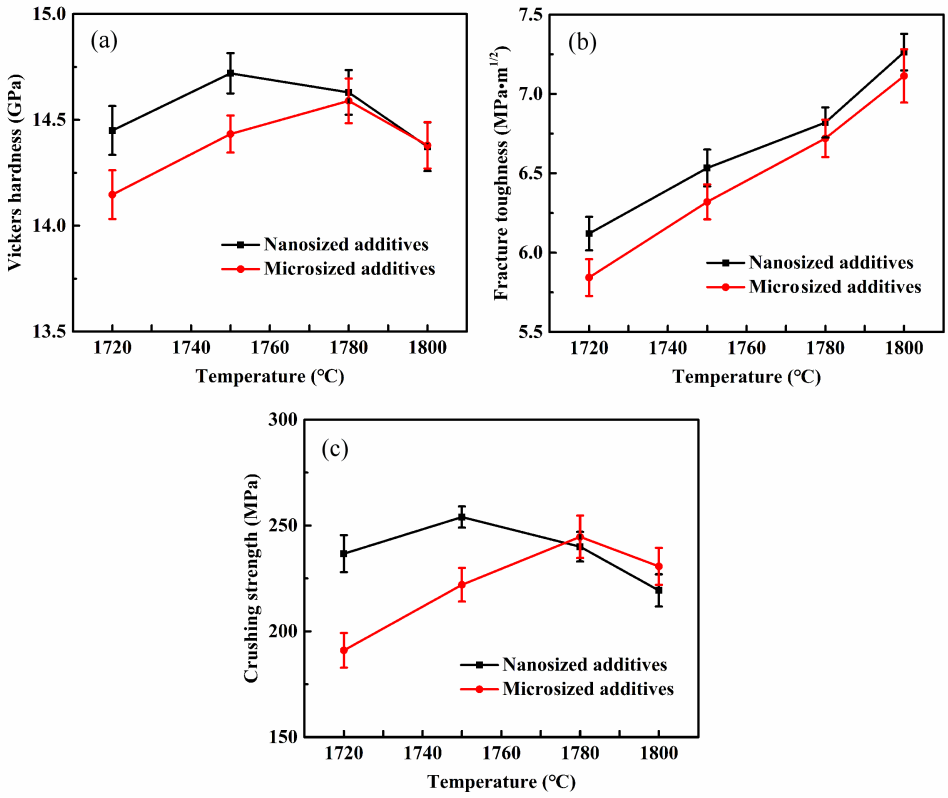

Figure 9. Mechanical properties of Si_3N_4 ceramic balls: a) Vickers hardness, b) indentation fracture toughness and c) crushing strength

Table 2. A comparison of the mechanical properties (Vicker hardness *HV*, indentation fracture toughness K_{IC} and crushing strength σ) obtained in the present work and relevant literature

Sintering additives (average particle size)	Sintering parameters	*HV* [GPa]	K_{IC} [MPa·m$^{1/2}$]	σ [MPa]	Ref.
5 wt.% Y_2O_3 (1.2 μm) + 5 wt.% Al_2O_3 (0.8 μm)	GPS/ 1780 °C/ 2 h/ 3 MPa	14.6	6.7	245	present work
5 wt.% Y_2O_3 (50 nm) + 5 wt.% Al_2O_3 (30 nm)	GPS/ 1750 °C/ 2 h/ 3 MPa	14.7	6.5	254	present work
3 wt.% Y_2O_3 (0.9 μm) + 3 wt.% Al_2O_3 (0.8 μm)	GPS/ 1800 °C/ 6 h/ 0.7 MPa + HIP/ 1700 °C/ 1 h/ 100 MPa	14.5	6.3	180	[31]
4 wt.% Nd_2O_3 + 4 wt.% Al_2O_3 + 4 wt.% La_2O_3	GPS/ 1750 °C/ 2 h + HIP/ 1750 °C/ 2 h	14.4	6.6	-	[32]

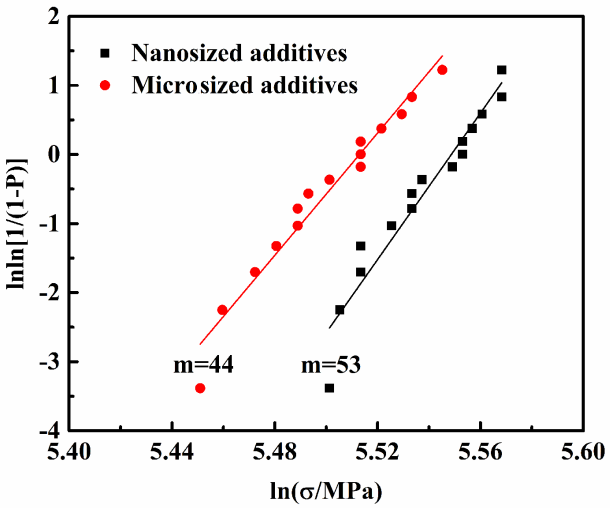

Figure 10. The Weibull distribution of crushing strength of Si_3N_4 ceramic balls: sample NSA at 1750 °C and sample MSA at 1780 °C

In general, the comprehensive mechanical properties of the sample NSA sintered at 1750 °C are optimal, with the Vickers hardness, indentation fracture toughness and crushing strength of 14.7 ± 0.1 GPa, 6.5 ± 0.1 MPa·m$^{1/2}$ and 254 ± 8.5 MPa, respectively. The mechanical properties obtained in the present work have been compared with the literature data, as shown in Table 2. It can be seen from Table 2 that the mechanical properties of the Si_3N_4 ceramic balls prepared in the present work are comparable to the data given in the literature.

Figure 10 shows the Weibull distribution of crushing strength of the Si_3N_4 ceramic balls with the microsized and nanosized sintering additives after sintering at the optimal temperature (1780 and 1750 °C, respectively). It can be seen from Fig. 10 that the Weibull modulus increases from 44 to 53, when the particle size of the Y_2O_3-Al_2O_3 additives changes from micron to nanometer scales, which indicates that the reliability of the Si_3N_4 ceramic balls is drastically improved by adding nanosized sintering additives.

IV. Conclusions

Gas-pressure-sintered Si_3N_4 ceramic balls with high reliability and excellent mechanical properties were successfully prepared by adding nanosized Y_2O_3-Al_2O_3 additives. The conclusions are summarized as follows:

i) The dispersion of the nanosized sintering additives in the Si_3N_4 matrix is more homogeneous than that of the microsized sintering additives, which promoted the densification of the Si_3N_4 ceramic balls at lower temperature. Obtained microstructure consists of β-Si_3N_4 grains with larger aspect ratio and more uniform grain size distribution when the nanosized additive is used. Such a microstructure is conducive for the improvement of mechanical properties of the Si_3N_4 ceramic balls.

ii) The Si_3N_4 ceramic balls with the nanosized sintering additives have the optimal comprehensive mechanical properties after sintering at 1750 °C, with Vickers hardness of 14.7 ± 0.1 GPa, indentation fracture toughness of 6.5 ± 0.1 MPa·m$^{1/2}$ and crushing strength of 254 ± 8.5 MPa.

iii) The Weibull modulus of crushing strength distribution of the Si_3N_4 ceramic balls with the nanosized sintering additives increases from 44 to 53, compared with the Si_3N_4 ceramic balls with the microsized sintering additives. This indicates that the nanosized sintering additive is beneficial to enhance the reliability of the Si_3N_4 ceramic balls.

References

1. V. Brizmer, A. Gabelli, C. Vieillard, G.E. Morales-Espejel, “An experimental and theoretical study of hybrid bearing micropitting performance under reduced lubrication”, *Tribol. Trans.*, **58** [5] (2015) 829–835.
2. G.T.Y. Wan, A. Gabelli, E. Ioannides, “Increased performance of hybrid bearings with silicon nitride balls”, *Tribol. Trans.*, **40** [4] (1997) 701–707.
3. M. Mosleh, K. Bradshaw, J.H. Belk, J.C. Waldrop, “Fatigue failure of all-steel and steel-silicon nitride rolling ball combinations”, *Wear*, **271** [9-10] (2011) 2471–2476.
4. P.J. Dempsey, J.M. Certo, W. Morales, “Current status of hybrid bearing damage detection”, *Tribol. Trans.*, **48** [3] (2005) 370–376.
5. M.H. Bocanegra-Bernal, B. Matovic, “Dense and near-net-shape fabrication of Si_3N_4 ceramics”, *Mater. Sci. Eng. A*, **500** [1] (2009) 130–149.
6. R.L. Satet, M.J. Hoffmann, R.M. Cannon, “Experimental evidence of the impact of rare-earth elements on particle growth and mechanical behaviour of silicon nitride”,

Mater. Sci. Eng. A, **422** [1] (2006) 66–76.
7. J. Tatami, E. Kodama, H. Watanabe, H. Nakano, T. Wakihara, T. Meguro, A. Azushima, "Fabrication and wear properties of TiN nanoparticle-dispersed Si_3N_4 ceramics", *J. Ceram. Soc. Jpn.*, **116** [1354] (2008) 749–754.
8. P.F. Becher, G.S. Painter, N. Shibata, S.B. Waters, H.T. Lin, "Effects of rare-earth (RE) intergranular adsorption on the phase transformation, microstructure evolution, and mechanical properties in silicon nitride with RE_2O_3 + MgO additives: RE = La, Gd, and Lu", *J. Am. Ceram. Soc.*, **91** [7] (2008) 2328–2336.
9. S. Li, C. Wei, L. Zhou, L. Sheng, Z.P. Xie, "Microstructure and fracture strength of silicon nitride ceramics consolidated by oscillatory pressure sintering", *Ceram. Int.*, **45** [12] (2019) 14235–14240.
10. Z.K. Hyang, A. Rosenflanz, I.W. Chen. "Pressureless sintering of Si_3N_4 ceramic using AlN and rare-earth oxides", *J. Am. Ceram. Soc.*, **80** [5] (2010) 1256–1262.
11. V. Demir, D.P. Thompson, "Pressureless sintering of Si3N4 ceramics with oxide additives in different packing powder", *J. Mater. Sci.*, **40** [7] (2005) 1763–1765.
12. S.Y. Yoon, T. Akatsu, E. Yasuda, "The microstructure and creep deformation of hot-pressed Si_3N_4 with different amounts of sintering additives", *J. Mater. Res.*, **11** [01] (1996) 120–126.
13. M.J. Hoffmann, A. Geyer, R. Oberacker, "Potential of the sinter-HIP-technique for the development of high-temperature resistant Si_3N_4-ceramics", *J. Eur. Ceram. Soc.*, **19** [13] (1999) 2359–2366.
14. M. Mitomo, N. Hirosaki, T. Nishimura, R.J. Xie, "Microstructure control in silicon nitride ceramics - A review", *J. Ceram. Soc. Jpn.*, **114** [1335] (2006) 867–872.
15. R.B. Greene, S. Fünfschilling, T. Fett, M.J. Hoffmann, J.J. Kruzic, J. Roedel, "Fatigue crack growth behavior of silicon nitride: roles of grain aspect ratio and intergranular film composition", *J. Am. Ceram. Soc.*, **96** [1] (2013) 259–265.
16. P. Ajgalik, J. Dusza, M.J. Hoffmann, "Relationship between microstructure, toughening mechanisms, and fracture toughness of reinforced silicon nitride ceramics", *J. Am. Ceram. Soc.*, **78** [10] (1995) 2619–2624.
17. A. Jayatilaka, K. Trustrum, "Statistical approach to brittle fracture", *J. Mater. Sci.*, **12** (1977) 1426–1430.
18. K. Trustrum, A. Jayatilaka, "Applicability of Weibull analysis for brittle materials", *J. Mater. Sci.*, **18** [9] (1983) 2765–2770.
19. S. Nakamura, S. Tanaka, R. Furushima, K. Sato, K. Uematsu, "Estimation of Weibull modulus from coarser defect distribution in dry-pressed alumina ceramics", *J. Ceram. Soc. Jpn.*, **117** [1366] (2009) 742–747.
20. G. Quinn, "Flexure strength of advanced structural ceramics: a round robin", *J. Am. Ceram. Soc.*, **73** [1990] 2374–2384.
21. K. Niihara, R. Morena, D.P.H. Hasselman, "Evaluation of K_{Ic} of brittle solids by the indentation method with low crack-to-indent ratios", *J. Mater. Sci. Lett.*, **1** (1982) 13–16.
22. P. Supancic, R. Danzer, W. Harrer, Z.H. Wang, S. Witschnig, O. Schoeppl, "Strength tests on silicon nitride balls", *Key Eng. Mater.*, **409** (2009) 193–200.
23. D.K. Shetty, V.K. Pujari, "Load-bearing capacity in quasi-static compression and bearing toughness of silicon nitride balls", *Tribol. Trans.*, **47** [4] (2004) 522–526.
24. H.D. Kim, B.D. Han, D.S. Park, B.T. Lee, P.F. Becher, "Novel two-step sintering process to obtain a bimodal microstructure in silicon nitride", *J. Am. Ceram. Soc.*, **85** [1] (2010) 245–252.
25. F.C. Peillon, F. Thevenot, "Grain coarsening in gas pressure sintered silicon nitride", *Ceram. Int.*, **28** [6] (2002) 637–643.
26. K. Jeong, J. Tatami, M. Iijima, T. Takahashi, "Fabrication of Si_3N_4 ceramics by postreaction sintering using Si-Y_2O_3-Al_2O_3 nanocomposite particles prepared by mechanical treatment", *Ceram. Int.*, **42** [10] (2016) 11554–11561.
27. A. Kumar, A. Gokhale, S. Ghosh, S. Aravindan, "Effect of nano-sized sintering additives on microstructure and mechanical properties of Si_3N_4 ceramics", *Mater. Sci. Eng. A*, **750** [18] (2019) 132–140.
28. S.I. Go, Y. Li, J.W. Ko, H.N. Kim, Y.J. Park, "Microstructure and thermal conductivity of sintered reaction-bonded silicon nitride: the particle size effects of MgO additive", *Adv. Mater. Sci. Eng.*, **2018** [4] (2018) 1–5.
29. F.L. Riley, "Silicon nitride and related materials", *J. Am. Ceram. Soc.*, **83** (2000) 245–265.
30. D. Green, *An Introduction to the Mechanical Properties of Ceramics*, Cambridge University Press, 1998, pp. 210–284.
31. M. Komatsu, M. Takao, "Wear resistant member comprised of silicon nitride and process for producing the same", *U.S. Patent 7521388 B2*, 2009.
32. V.K. Pujari, W.T. Collins, "Silicon nitride body and method of manufacture", *U.S. Patent 20080150199 A1*, 2008.